Available online at www.sciencedirect.com
SCIENCE DIRECT
Acta Materialia 54 (2006) 729–742
Acta MATERIALIA
www.actamat-journals.com

Development of a generalized parameter window for cold spray deposition

Tobias Schmidt *, Frank Gärtner, Hamid Assadi [1], Heinrich Kreye

Helmut Schmidt University, University of the Federal Armed Forces Hamburg, Holstenhofweg 85, D-22043 Hamburg, Germany

Received 24 February 2005; received in revised form 4 October 2005; accepted 5 October 2005
Available online 1 December 2005

Abstract

In cold spraying, bonding occurs when the impact velocities of particles exceed a critical value. This critical velocity depends not only on the type of spray material, but also on the powder quality, the particle size and the particle impact temperature. Bonding in cold spraying is associated with adiabatic shear instabilities caused by high strain rate deformation during impact. Numerical and experimental methods are developed to investigate the influence of impact conditions and related phenomena on the coating quality. For a quantitative analysis, the materials behaviour was investigated through spray experiments, which were complemented by ballistic impact tests and explosive powder compaction. In this way, impact dynamics, bonding mechanism and critical velocities are linked to develop a general formulation, incorporating material properties and particle size, for the prediction of required impact conditions for cold spray deposition.

Keywords: Cold spraying; Particle impact; Modelling; Bonding; Shear instability

1. Introduction

In cold spraying, particles are accelerated in a preheated high-pressure gas stream passing through a DeLaval type nozzle before they impact the substrate. In contrast to conventional thermal spraying, particles are only slightly heated prior to impact. The impact velocities range from 200 to 1200 m/s, depending on nozzle geometry, particle size and shape, and the type, temperature and pressure of the process gas. Under optimised conditions, the impacting particles form a dense coating with low oxide content. Bonding in cold spraying results from particle deformation during impact, which is influenced by impact conditions and various powder characteristics.

Optimisation of coating microstructure and coating properties, for each combination of substrate and coating materials, calls for a series of spray experiments and respective characterisation. Without an adequate understanding of the mechanisms of bonding and coating formation, however, such optimisations can be excessively time consuming and costly – if at all feasible. The desire to tune cold spraying for particular materials has thus motivated studies of bonding mechanisms. The main characteristics of bonding in cold spraying can be compared to those in processes such as explosive welding or shock wave powder compaction [1,2]. In all of these processes, bonding is achieved when a critical impact velocity is exceeded. The critical velocity in these processes is perceived generally to be a function of material properties [3,4].

In cold spraying, successful bonding of an impacting particle requires localized deformation and adiabatic shear instabilities, which occur at sufficiently high impact velocities, the so called critical velocity [1–3,5]. Numerical analyses are able to indicate shear instabilities and thus provide a basis for the calculation of the critical velocity in terms of materials properties and process parameters. Assadi et al. [1] have used numerical simulation to work out the effect

* Corresponding author. Tel.: +49 40 6541 2129; fax: +49 40 6541 2006.
E-mail address: tobias.schmidt@hsu-hh.de (T. Schmidt).
[1] On leave from Tarbiat Modarres University, Tehran, Iran.

1359-6454/$30.00
doi:10.1016/j.actamat.2005.10.005

Table 1
Nomenclature, use SI-units for calculation

c_p	Specific heat
d, x	Diameter, distance
F_1, F_2	Empirical factors
T_i	Impact temperature
T_m	Melting temperature
T_R	Reference temperature (293 K)
t	Time
v	Velocity
ρ	Density
σ_U	Yield stress
σ_{TS}	Tensile strength
λ	Thermal conductivity

of various material properties on the critical velocity in cold spraying. They summarised these effects into a simple expression for the critical velocity (here presented in SI units) as follows:

$$v_{crit} = 667 - 0.014\rho + 0.08(T_m - T_R) + 10^{-7}\sigma_u - 0.4(T_i - T_R) \quad (1)$$

with the parameters defined in Table 1. Eq. (1) can be used to estimate the influence of only small changes in material and process parameters on the critical velocity, and is thus limited to materials with properties similar to those of the reference material, i.e., copper.

The work of Assadi et al. does not consider the size of particle as an influential factor. However, a couple of reports suggest that the size of impacting particles may influence the critical velocity [6–9]. One possible origin of critical velocities varying with particle size could be the different surface to volume ratio taking into account mainly the higher amount of adsorbents or oxides of smaller size fractions hindering bonding. The length scales of heat conduction and size dependent differences in strain rate hardening can give other explanations. One aim of the present study was to quantify these different effects and to describe the influences of particle size on the critical velocity. Additionally, effects of general materials properties and particle impact temperatures on the critical velocity were reviewed and summarised into new simple relations. These relations were used as more comprehensive guidelines to facilitate optimisation of the cold spray process for various spray materials.

For a deeper understanding of impact phenomena and coating formation, the particle impact was modelled by using the finite element software ABAQUS/Explicit. For most materials, high-strain-rate data are not available. Therefore, materials behaviour under high strain rate deformation was investigated and verified by cold spraying and selected experiments of single impacts and powder compaction. Results from these experiments in turn were used to tune parameters for modelling. Each of these different methods makes an individual and irreplaceable contribution to complete the overview of different impact phenomena.

2. Methods

2.1. Numerical simulations

For a fundamental investigation of impact phenomena, especially particle bonding, and to study the influence of material properties on these phenomena, the interaction of particles with substrates was modelled by using the commercial Lagrangian finite element program ABAQUS/Explicit [10]. Using an axisymmetric model, single particles are assumed to impact the substrate in normal direction with given impact velocity and temperature. The Mie–Grüneisen equations of state were used to model elastic material behaviour. The Johnson–Cook model was used to describe the plastic flow of material, which is influenced by strain-hardening, strain-rate-hardening, and thermal softening [11,12]. It was assumed that 90% of the plastic strain energy dissipates into heat. The calculations were performed for different particle sizes as a dynamic explicit procedure including thermal displacement. The thermal conductivity of the highly deformed material was assumed to be 60% of that of the annealed bulk material. It should be noted, however, that in the case of very small dimensions or when the rate of heat propagation approaches the speed of sound, the diffusive heat equation is no longer valid. In this case, wave propagation might be the dominating heat transfer mechanism [1,13]. However, this condition was never encountered in the present study.

Copper was chosen as a suitable example for the calculations, considering the fact that it is a widely used spray material for which reliable high-strain-rate material data are available [11,12]. But even for copper, high-strain-rate data are only available for strain-rates of up to 10^6/s, whereas the maximum strain-rates in cold spraying can be in the range of 10^9/s, e.g., for a particle 10 μm in diameter impacting at 600 m/s. The simple logarithmic approximation of strain-rate-hardening in the Johnson–Cook model was extended to this range, but will probably not be able to describe strain-rate-hardening precisely over that wide range of extrapolation. Nevertheless, for most materials, this approximation supplies a reasonable description of high-stain-rate deformation. However, for some others the extrapolation can lead to some uncertainties, such as for steel 316L which shows an increase of strain-rate-hardening in the range between 10^6 and 10^9/s (see Section 3.5).

2.2. Cold spray and explosive powder compaction experiments

Details of cold spraying and the experimental set-up are given elsewhere [3,4]. In order to study the influence of particle size on the critical velocity and coating quality, copper and steel 316L powders of various size distributions were used. For each set of spray parameters, the deposition efficiency (DE) was measured by relating the weight increase of coated substrates to the respective powder mass flow. Critical velocities were determined by correlating particle size

distributions and deposition efficiencies. Since the velocity of a particle is a function of its size, the amount of adhering material can be correlated to the respective size distribution of a particular powder. Using a powder with negligible amounts of fine particles, the critical velocity for bonding can be worked out as the velocity of the largest particle which adheres to the substrate. Respective particle impact velocities and temperatures were calculated by using fluid dynamic and heat transfer calculations. Previous investigations demonstrated that this approach supplies reliable data [3]. Details of respective procedures are given in [3,4]. In order to cover a wide range of impact conditions, nozzles of different lengths were used with nitrogen or helium as process gas. Subsequently, coating microstructures and coating properties were investigated by optical microscopy (OM), scanning electron microscopy (SEM) and tensile tests. Moreover, the effect of impact temperature on bonding was assessed experimentally for copper, through tensile tests of various coatings, processed with powders of different size distributions.

Bonding by high-strain-rate deformation can also be studied by explosive powder compaction [2,14–18]. Particle bonding in this process can be linked to that in cold spraying, by appropriate consideration of the particle loading mechanics in the two methods. In explosive compaction, the powder is loaded by a strong shock wave. The shock wave causes a discontinuous pressure jump up to the shock pressure in the shock front. The shock front propagates through the powder with shock velocity, so that the powder is accelerated and deformed at high-strain-rates. In the present study, explosive powder compaction was performed by the so-called direct method, which again is described elsewhere [2,14,15]. The advantage of this method is that powder can be tested under a wide range of loading conditions in one single experiment, i.e., giving equivalent impact velocities in the range of 400–1500 m/s in one sample. Moreover, the particle load in explosive powder compaction is independent of particle size and particle shape. It only depends on the apparent powder density and the boundary loading conditions, which are easy to determine. The particle temperature prior to impact is constant and well known for all particles. Under- and overcritical loading conditions cause characteristic deformation patterns – i.e., 'angular' and 'parachute-like' shapes, respectively – which can be easily distinguished from one another [2]. This latter merit makes powder compaction a particularly attractive method for determining critical velocities for various materials and investigating the influence of particle size on bonding. Critical velocities in explosive powder compaction were determined by correlating the transition of microstructural features or abrupt changes of the local cavitation resistance according to particle erosion with the dynamic load at the respective sample radius [2].

2.3. Single impacts

Single impacts during spray experiments can be produced by the so-called wipe-tests, in which a polished substrate is moved rapidly through the spray jet. Subsequently, SEM can be used to investigate the morphology of impacted particles. A disadvantage of this method is that the exact velocity and temperature of the individual particles upon impact are not known. Additionally, thorough investigation of the interfacial features can be difficult for small particles.

To ensure a well-defined condition for single impacts, a scaled-up test was developed as follows. A 20-mm gun was used to accelerate a bullet, which consisted of a metal ball and a polymer driving plug. The driving plug and metal ball separate after leaving the barrel. The impact velocity of the ball was measured by a photo-electric barrier. Metal balls with diameters of 20 mm were accelerated to velocities ranging from 200 to 1500 m/s, comparable to that of cold-sprayed particles. In this way, the dynamic material behaviour and bonding of different combinations of materials were investigated in an enlarged scale under well-known impact conditions. From such macro impacts, the DE was determined as the ratio between the mass of the impacting spheres and substrates and respective mass after impact.

2.4. Analysis of microstructure and properties

The powder morphologies of the feedstock materials were analysed by SEM. Cross sections of coatings as well as cross-sections from the scaled-up 20 mm single impact tests were investigated by OM in as-polished and as-etched conditions. Spectrometric methods using a commercial analyzer of the type Leco TC300 were applied for the quantitative analysis of the oxygen and the nitrogen contents of feedstock material and coatings. Hardness measurements were performed on polished cross-sections of feedstock powders, coatings and compacts using a Vickers indenter. The particle–particle adhesion strength of the compacts was tested by a modified ASTM G32 cavitation test [19]. The interfacial bond strength of the scaled-up single impacts was investigated by shear tests for which segments with sizes of $4\,\text{mm} \times 4\,\text{mm}$ were prepared out from the bonded zone at the crater sides and the south pole region of the impact crater.

To evaluate differences in bonding quality, the tensile strength of cold-sprayed coatings was determined by a customised tensile test of coated cylindrical specimens – referred to here as the tubular coating test (TCT). These tests are easy to perform routinely and can hence supply information on coating quality in addition to the microstructural investigations. In order to make tubular specimens, two cylindrical substrates are fixed face to face by a screwable holder, and the assembly is then fixed to a lathe chuck. The assembly of substrates remain in this fixed position during further preparation and during the coating process. For the present analysis, cylinder sizes of 25 mm in diameter and 25 mm in length were used with respect to standards for bond strength tests (EN 582 or ASTM C633). To ensure high bond strengths, AlMg3 was chosen

as the substrate material [3]. After fixing the substrates to the holder, the cylindrical shell was machined to a roughness of less than 40 μm, to clean the surface and to ensure that there was no gap between the two cylinders.

The assembled substrate was then coated with typical kinematic parameters with respect to radial and axial advance, and powder feed rates. Coatings with thickness between 500 and 1000 μm were prepared for that test. The strength of TCT specimens was then measured by using the equipment for bond strength test at the tensile machine. As in bond strength tests, three TCT samples were tested for each set of parameters. It is worth noting that the discontinuity in the assembly of substrates leads to a stress concentration in the coating (notch effect) during the test. A finite element stress analysis of the specimen shows that this stress concentration increases the von Mises stress by a factor of 1.5 at the gap between the two substrates. This factor should be taken into account in quantitative analyses of coating strength.

Investigations of microstructures, the DE and tensile tests were used as standard procedures, when optimising the cold spray process for new materials.

3. Results and discussion

3.1. Numerical analysis of size effect

Numerical simulations of the particle impact were performed to obtain information about the impact loading of the particles concerning the local distribution and the temporal evolution of pressure, stress, strain and temperature. With the beginning of the impact, a strong pressure field propagates spherically into the particle and substrate from the point of first contract, Fig. 1(a). The pressure gradient at the gap between the colliding interfaces generates a shear load, which accelerates the material laterally and thereby causes localized shear straining. When the impact pressure and the respective deformation are high enough, this shear straining leads to adiabatic shear instabilities. This means that thermal softening is locally dominant over strain and strain-rate hardening, which leads to a discontinuous jump in strain and temperature and an immediate breakdown of stress. The viscous flow in this region generates an out-flowing material jet with material temperatures close to the melting temperature, Fig. 1(b). This phenomenon of jetting is also a known feature in explosive cladding of materials [6,20]. At the highly strained interfaces, oxide shells are broken and the heated surfaces are pressed together and are thus bonded. In cold spraying, in particular, ductility is needed to obtain sufficient flattening of particles in order to build up a dense coating. According to the simulations, the material deformation can reach strain-rates in the bond zone of up to 10^9/s and strains of 10 or even more. A 'sprayable' material should withstand such severe conditions of plastic flow without fracturing. The simulations also give an estimate of the heating and cooling rates. The cooling rate is a particularly important factor: in the bond zone, it should on one hand be low enough to promote shear instability, and high enough, on the other hand, to let the interface solidify and complete the bonding process, before the particle bounces back. Moreover, the bond strength should be high enough to withstand elastic 'spring-back' forces to avoid particle detachment.

Analytical descriptions for material deformation and heat transfer already indicate that sizes can play a role for attainable interface temperatures, strain rates and stress. For very small dimensions, the occurrence of shear instabilities can be hindered by high cooling rates, which arise due to very high temperature gradients within a small particle. In addition, the strain-rate is higher and hence strain-rate hardening can be more profound in smaller particles. Also the viscous shear strength in the jetting region will be higher for smaller dimensions. All these dynamic effects hinder localized deformation and thus increase critical velocity. Moreover, smaller particles are exposed to higher quench rates during powder production and show an intrinsically higher strength because of their finer microstructure (e.g., Hall–Petch hardening). Due to their higher surface to volume ratios, smaller particles often have a higher impurity content. Surface contaminations such as oxide shells will have a significant influence on bonding. All these effects can lead to an increased critical velocity for finer particles.

In the present work, both heat conduction and strain-rate-hardening effects are incorporated into the numerical analysis. Fig. 2 shows the plastic strain field of 5 and 50 μm copper particles, both of which impacted at 600 m/s on a copper substrate. The grey-scale indicates straining from 0.1 to 5. As shown in the figure, the required localized deformation at the particle–substrate interface is missing for the 5 μm particle. A more quantitative analysis focuses on the temporal evolution of temperature, represented as the average temperature of the elements in the highly

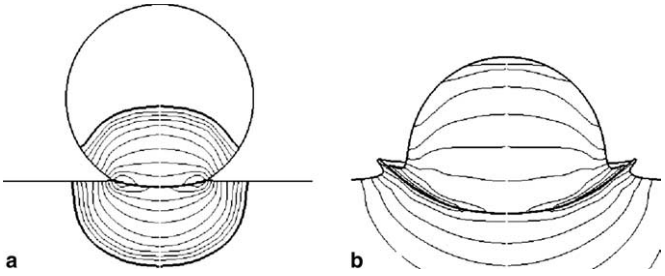

Fig. 1. Pressure field during impact (a), jetting (b).

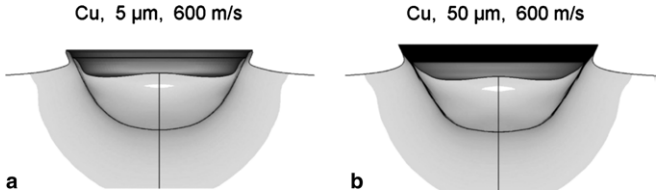

Fig. 2. Plastic strain field plot of a 5 μm (a) and 50 μm (b) copper particle which impacted at 600 m/s.

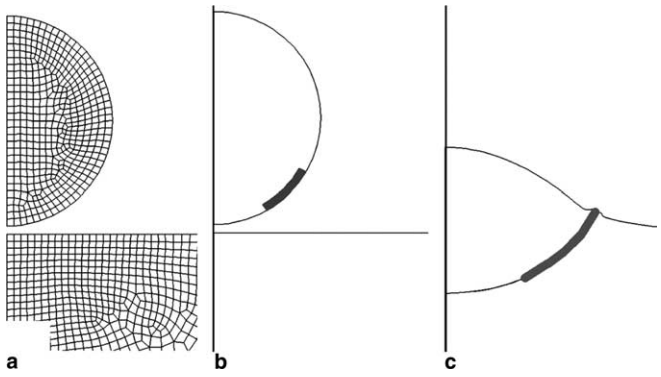

Fig. 3. Axisymmetric mesh (a), mesh set for monitoring the temporal evolution of temperature in pre- (b) and post-impact state (c).

strained contact zone. Fig. 3 shows the initial mesh (Fig. 3(a)) and the selected elements (Fig. 3(b)) to monitor temperature. The highly strained contact zone under well bonded conditions can amount up to more than 80% of the contact area in the post-impact state, Fig. 3(c). Adiabatic shear instabilities are detected by the occurrence of a jump in the temporal evolution. Fig. 4 shows the temporal evolution of temperature for copper particles of different size and impact velocities of 400, 500 and 600 m/s. The shift of the temperature rise to shorter times with increasing velocities can be attributed to the higher load and the faster propagation of the load within spray particles. For the 5 μm particles, no shear instabilities could be detected. The average temperature at the selected part of the interface is only slightly increased and even higher impact velocities do not lead to shear instabilities. The fast rate of heat transfer over the particle volume, in these small dimensions, prevents the occurrence of localized shear instabilities. The 15 μm particle shows a sudden temperature rise, indicating shear instabilities which occur at velocities of 500 m/s or above that. The maximum average temperature of the selected volume reaches 820 K for an impact velocity of 600 m/s. The 25 and 50 μm particles show a temperature rise and shear instability at the particle–substrate interface for 500 and 600 m/s, respectively. In all cases, where shear instability is encountered, the peak temperature increases with impact velocity asymptotically up to the melting point. For the 25 and 50 μm particles, at impact velocity of 600 m/s, the maximum temperatures are close to the melting temperature of copper. The cooling rate decreases with increasing particle size. At an interface temperature of 750 K the cooling rate for the 15 μm particle is 20×10^9 K/s, for the 25 μm particle 5×10^9 K/s and for the 50 μm particle 1×10^9 K/s. The ratio of heating rate to cooling rate in this case is 2.5 for the 15 μm particle, 28 for the 25 μm particle and 70 for the 50 μm particle. This shows that the so called adiabatic shear instabilities can not be assumed to be adiabatic in these small dimensions,

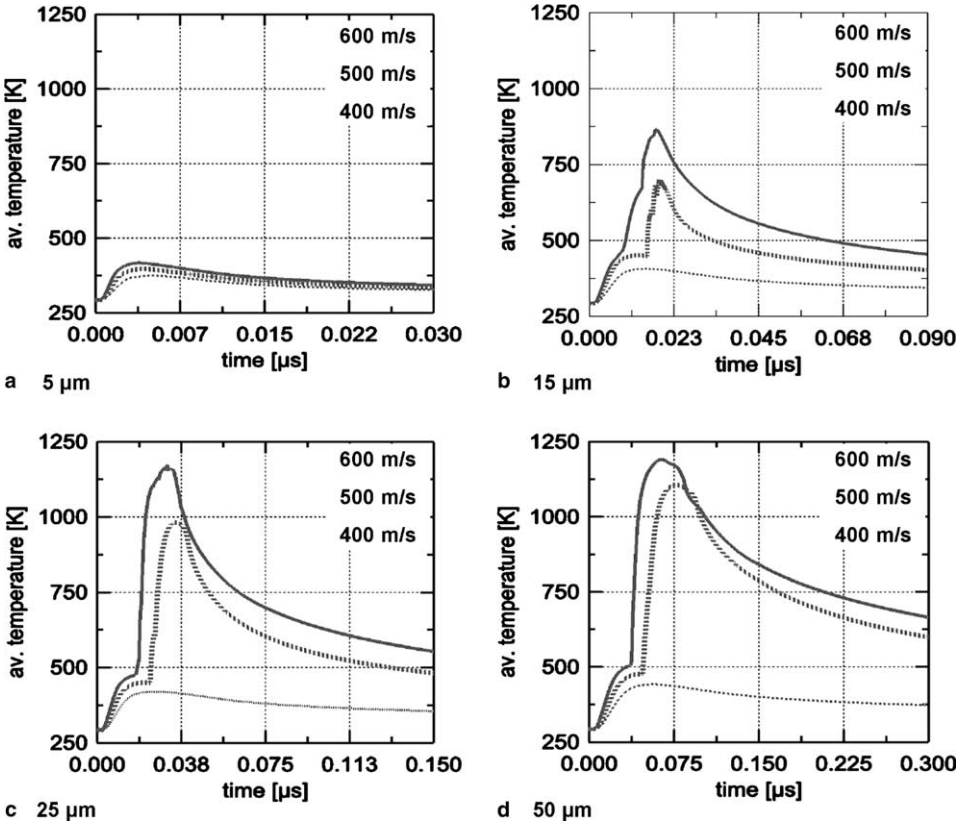

Fig. 4. Temporal evolution of the temperature at the monitored volume (sheared interface) of copper particles of different size and for different impact velocities.

but the occurrence of these shear instabilities needs sufficient adiabatic straining. If the cooling rate in the highly strained regions comes close to the heating rate, shear instabilities are hindered or prevented completely.

Overall, for very small particles the compensation of the generated heat is extremely fast and hence the maximum interface temperatures are significantly lower than those of coarser particles. Very small particles show no indication of shear instability. On the other hand, maximum interface temperatures in coarser particles, with sufficiently high impact velocities, are close to the melting temperature. Because of the lower cooling rates, their interfaces are exposed to high temperatures for longer times. Considering particle bonding as a diffusion process, the bonding quality should be influenced by the thermal history of the contact zone and perhaps by contact pressure. The occurrence of a sufficient amount of shear instabilities is monitored by using a threshold that 20% of the particle–substrate interfaces are exceeding a temperature of more than 1000 K. That criterion for bonding was used to determine critical velocities. In these numerical analyses, velocities were increased in steps of 50 m/s to cover a range from 300 to 800 m/s. For different Cu-particle sizes, the results of the temporal evolution of the temperature at particle interfaces can be interpreted as follows. At feasibly high impact velocities, a 5 μm particle does not bond to the substrate, although it might be entangled into it. A 15 μm particle bonds at 600 m/s, a 25 μm particle at 500 m/s, and a 50 μm particle at 450 m/s. The calculated size-dependent critical velocities show a suitable agreement to experimentally determined values presented in Section 3.4 by Eqs. (9) and (10).

Fig. 5(a) shows the temporal evolution of temperature for Cu-particles of different sizes, impacting on Cu-substrate with a velocity of 600 m/s at a initial impact temperature of 20 °C. The stretched time scales for increased particle sizes can be attributed to the different times required for the deformation wave reaching the monitored volume and propagating through it. These results demonstrate that bonding quality will increase with particle size under the same impact velocities, because maximum temperature and the corresponding 'bonding time' are both increased. Fig. 5(b) shows the temporal evolution of interface temperature for a 25 μm copper particle impacting to a copper substrate with 600 m/s, calculated for different initial temperatures. The increase of initial particle and substrate temperature increases the interface peak temperature and furthermore significantly increases the high temperature time scale. Higher initial particle temperatures result in lower critical velocities. That is due to the facts that the material is already softer at higher temperatures and that less kinetic energy is needed to heat particle surface areas by plastic deformation. Moreover, heat conduction will be less effective due to lower temperature gradients, which leave more time for diffusion and bonding. Thus, the coating quality can be further improved by increasing the initial temperatures of particles and substrates.

It is worth noting here, that similar numerical investigations were also performed for other spray materials. For the examples of Cu and steel 316L, in particular, the results from modelling impacts were subsequently verified by experimental investigations. As shown later in Section 3.4, the effect of particle impact conditions with respect to particle sizes, temperatures and velocities, varied by using different spray powders and parameter settings, were studied by microstructural analyses and quantified by tensile tests.

3.2. Analytical estimation of size dependent effects

The numerical simulations demonstrate clearly that heat conduction can have a strong influence on bonding in cold spraying. This effect can also be expressed analytically as follows. The depth of heat diffusion can be estimated by Eq. (2), where Δt is the characteristic time scale calculated from particle diameter and given impact velocity, and x is the characteristic length, which depends on particle diameter. Respective values are obtained by taking the analytically determined critical impact velocity of a particle with

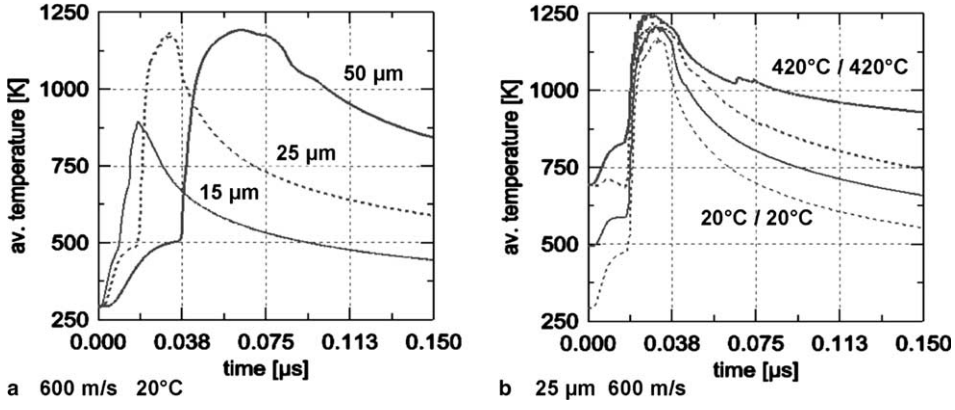

Fig. 5. Temporal evolution of the temperature at the monitored volume (sheared interface) of copper particles. Comparison of time scale and temperature for different particle sizes (a) and for different initial particle/substrate temperatures: 20 °C/20 °C, 220 °C/20 °C, 420 °C/20 °C, 420 °C/420 °C.

25 μm in diameter as impact velocity (see Section 3.3). The material dependent velocity for bonding should be close to this value. The characteristic length was taken as an arbitrary fraction of particle diameter and is used to calibrate this equation. Solving Eq. (2) for the particle diameter leads to Eq. (3):

$$x = \sqrt{\kappa \cdot \Delta t}, \quad \kappa = \frac{\lambda}{c_p \cdot \rho}, \quad \Delta t = \frac{d_{particle}}{v_{particle}}, \quad x = \frac{d_{particle}}{6}, \tag{2}$$

$$d_{crit} = 36 \cdot \frac{\lambda}{c_p \cdot \rho \cdot v_{particle}}. \tag{3}$$

This equation signifies a 'critical' particle diameter, above which thermal diffusion is slow enough to allow localized shear instability to occur at the surface of an impacting spherical particle. This means that smaller particles would not reach conditions for bonding. Fig. 6 shows calculated minimum diameters for selected metals. These values indicate that for tin, copper, silver and gold, thermal diffusion limits bonding of small particles, whereas spraying of titanium and steel 316L is less restricted by this effect.

3.3. Influence of particle properties on bonding conditions

From numerical calculations and cold spray experiments, it is already known that materials properties can have substantial influences on the critical velocity in cold spraying [1,3,6]. The aim of the following analysis is to develop simple equations, which predict impact dynamic effects, such as particle bonding or erosion, based on available materials data. It is assumed that particle and substrate materials as well as initial temperature are identical. Impact dynamic effects are determined by the interplay between material strength and dynamic load. On the left side of Eq. (4), the tensile strength is combined with the Johnson–Cook equation for thermal softening, to represent the temperature-dependent strength of material. On the right side, a ballistic expression for the crater ground pressure in hydrodynamic penetration is used, which characterizes the dynamic load. After introducing the calibration factor F_1, the equation is solved for velocity, which gives Eq. (5). This equation provides a mechanical balance of an impact:

$$F_1 \cdot \sigma_{TS} \cdot \left(1 - \frac{T_i - T_R}{T_m - T_R}\right) = \frac{1}{8} \cdot \rho \cdot v_{crit}^2, \tag{4}$$

$$v^{mech} = \sqrt{\frac{F_1 \cdot 8 \cdot \sigma_{TS} \cdot \left(1 - \frac{T_i - T_R}{T_m - T_R}\right)}{\rho}}. \tag{5}$$

Some impact effects will also depend on the energy balance between thermal dissipation and provided kinetic energy, which can be linked by a correlation factor F_2. This leads to Eq. (6), which contains the energy balance of an impact. Solving Eq. (6) for velocity leads to Eq. (7). The combination of Eqs. (5) and (7) by using a weight factor of 0.5 for both leads to Eq. (8), which matches better with experimental results than Eq. (5) or (7) on their own. The calibration factors ($F_1 = 1.2$, $F_2 = 0.3$) were generated by correlating calculated critical velocities on the basis of materials properties with experimentally determined critical velocities. The materials data were taken from [21–23]. It is worth noting, that such tabled data represent a certain mechanical and thermal history of the respective material and leave a range of uncertainty with respect to the properties of a spray powder. Thus, there is not much sense in supplying more exact values for the mechanical and the thermal calibration factor, F_1 and F_2, respectively. Fig. 7 shows the results for the calculation of critical impact velocities for 25 μm particles of different metals. In Fig. 8, calculated and experimentally determined critical impact velocities are compared for cold spraying and for 20 mm ball impacts. The correlation is much better than by using Eq. (1), especially with respect to tin and tantalum, which have significantly different properties than copper. The difference between v_{crit} of copper calculated with Eqs. (1) and (8) is based on differences in calibration data, in terms of particle size. With experimentally determined hardness values of spray powders, the tensile strength in Eq. (8) can also be replaced by the Vickers hardness to estimate critical

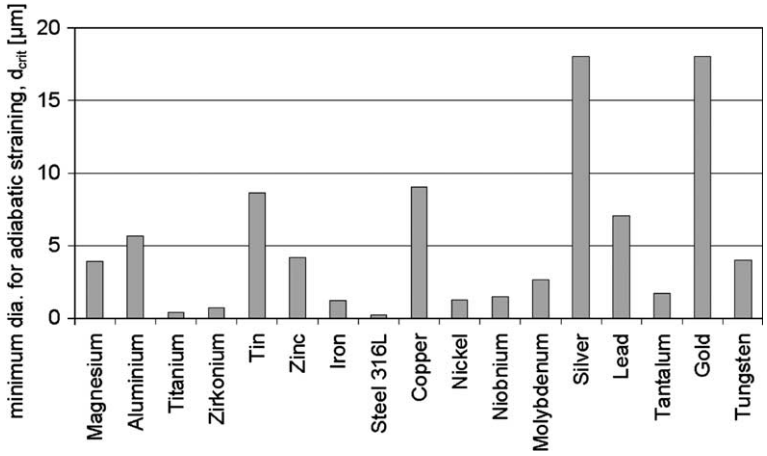

Fig. 6. Minimum particle diameter for localized adiabatic straining during impact calculated for different materials with semi-empirical Eq. (3).

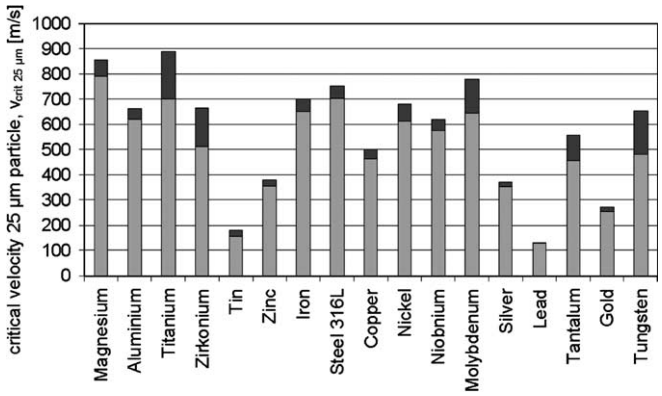

Fig. 7. Critical impact velocity for a 25 µm particle calculated for different materials with Eq. (8). The dark grey levels indicate a range of uncertainty with respect to the range of available materials data.

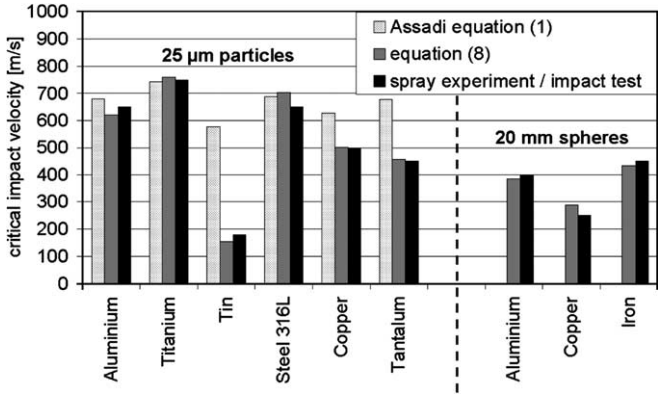

Fig. 8. Comparison of calculated v_{crit} with experimental results of spray experiments and impact tests.

velocity (here with $F_1 = 3.8$ and same thermal correlation factor $F_2 = 0.3$):

$$F_2 \cdot c_p \cdot (T_m - T_i) = \frac{1}{2} \cdot v_{crit}^2, \tag{6}$$

$$v^{th} = \sqrt{2 \cdot F_2 \cdot c_p \cdot (T_m - T_i)}, \tag{7}$$

$$v_{crit}^{th,mech} = \sqrt{\frac{F_1 \cdot 4 \cdot \sigma_{TS} \cdot \left(1 - \frac{T_i - T_R}{T_m - T_R}\right)}{\rho} + F_2 \cdot c_p \cdot (T_m - T_i)}. \tag{8}$$

There is one more impact effect, which can be very important for cold spraying. If the impact velocity is further increased, the plastic impact shows a transition to hydrodynamic penetration. In this case, the impacting particles will cause strong erosion. The material and temperature dependent velocity, where deposition changes to erosion, is here called the erosion velocity. As for bonding, material erosion can also be attributed to shear instabilities under ultra high loads. Respectively, the mechanical and the thermal balance can be considered as already expressed in Eq. (8). As described later in Section 3.5, the limit for erosion by particle penetration was experimentally determined by impact tests. The calibration factors F_1 and F_2 were determined by correlating that experimental results with calculations. Conditions for erosion can be estimated with Eq. (8) by using $F_1 = 4.8$ and $F_2 = 1.2$. Fig. 9 shows calculated erosion velocities for different metals. In cold spraying this range can be reached with lead, tin, gold, silver, zinc and under extreme spray conditions also with copper.

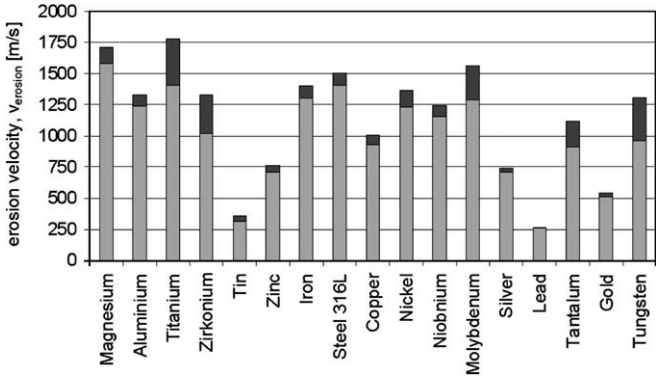

Fig. 9. Erosion velocity of different materials calculated with Eq. (8).

Finally it should be noted that the equations presented here only supply an estimation of the velocity range where impact effects such as bonding or erosion occur. As mentioned before, high-strain-rate and size effects as well as the powder purity, which are not included in these equations, can have a significant influence on impact dynamics. The mechanical part of these effects could ideally be integrated into the first term of Eq. (8) and the thermal part into the second term of Eq. (8), after obtaining a deeper understanding concerning their influence on bonding or erosion.

3.4. The window of sprayability

So far, critical velocities and erosion velocities were calculated for room temperature (20 °C). As mentioned earlier, the particle temperature in the cold spray process can be significantly higher. Moreover, almost all influential factors are temperature dependent, as described in Sections 3.1 and 3.3. The effect of temperature can be calculated using Eq. (8). Fig. 10 shows in a schematic sketch how v_{crit} and $v_{erosion}$ vary with temperature. The area under v_{crit} signifies the lack of bonding or slight erosion. The area above $v_{erosion}$ denotes strong erosion or, in the case of soft particles hitting a hard substrate, no deposition. The area between v_{crit} and $v_{erosion}$ describes the window of sprayability, WS, which can additionally be limited by a region of brittle material behaviour or limited ductility at lower temperatures. In the WS region, most of the impacting particles deposit as coating on the substrate. The particle impact conditions, PIC, describe particle velocity and particle temperature distributions for the chosen set of spray parameters (circle in Fig. 10). In this way, cold spraying can be optimised by tuning PIC for a maximum overlap with WS. The current

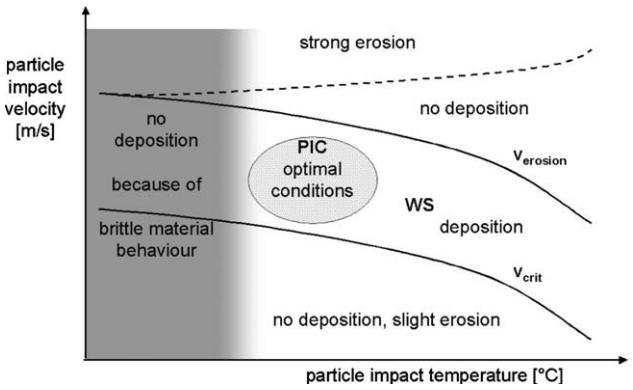

Fig. 10. Particle velocity over particle temperature with window of sprayability (WS) and the regime of particle impact conditions (PIC).

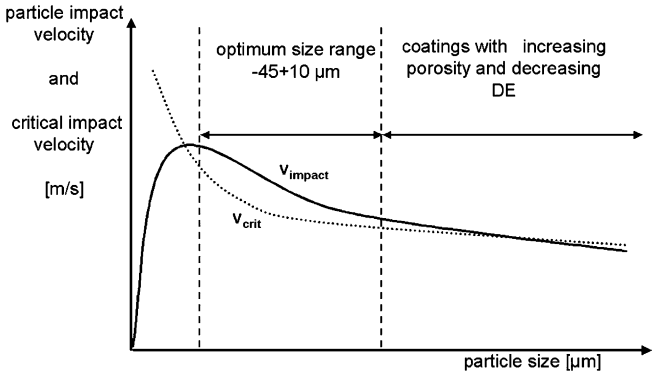

Fig. 11. v_{crit} and v_{impact} over particle size. Optimum particle size distribution for cold spraying.

analysis is an attempt to achieve this goal with a minimum number of trial-and-error experiments.

Fig. 10 shows schematically that WS could have a low-temperature limit, below which the material becomes brittle. For example, tin transforms at 13 °C from a brittle cubic diamond phase to a more ductile tetragonal phase; so it can only be sprayed with particle impact temperatures significantly higher than 13 °C. Together with the low melting temperature of tin ($T_m = 232$ °C), and a low strength, spray conditions are limited to a temperature range between 50 and 200 °C and a comparatively small window of particle velocities. For a particle temperature of 50 °C the particle velocity should be in the range of 150–340 m/s and for a particle temperature of 200 °C in the range of 70–150 m/s. This narrow window of sprayability was also experimentally approved for tin, by cold spray experiments using DE as a measure of WS. Body-centred cubic metals typically show a brittle-to-ductile transition on exceeding a certain temperature, T_{trans}. As a general rule, the impact temperature should be significantly higher than this temperature. Whereas tantalum ($T_{trans} = -270$ °C), niobium ($T_{trans} = -140$ °C) and iron ($T_{trans} = -30$ °C) are sprayable under standard cold spray conditions, molybdenum ($T_{trans} = 30$ °C) and tungsten ($T_{trans} = 300$ °C) show brittle behaviour and no deposition under such conditions, most probably because of a too low particle temperature.

Since the critical velocity for bonding is size-dependent, an additional optimisation is needed to determine optimum particle size distributions for each spray material. Using computational fluid dynamics, particle impact conditions PIC (particle temperature and velocity) at the substrate were calculated. The calculations also considered particle deceleration in the bow-shock at the substrate. Under standard conditions (N_2, 30 bar, 300 °C), Al-particles reach maximum v_{impact} at 15 µm, Cu-particles at 6 µm and Ta-particles at 4 µm. The effect of size on the critical velocity can be expressed for copper and steel 316L as follows ($T_i = 20$ °C, particle size range: 5–200 µm):

$$v_{crit}^{Cu} = 900 \cdot d_{particle}^{-0.19}, \quad (9)$$

$$v_{crit}^{316L} = 950 \cdot d_{particle}^{-0.14}. \quad (10)$$

The Eqs. (9) and (10) summarize the critical velocity measurements of cold spraying and explosive powder compaction experiments [1–3,9]. Fig. 11 shows a schematic of particle velocity and v_{crit} over particle size. Considering the size dependence of critical velocity, for most materials, there will be an optimum size range where v_{impact} is significantly higher than v_{crit}. On the left hand side of this range, there would be no deposition or insufficient bonding. On the right hand side of this range, v_{crit} and v_{impact} are nearly parallel, which leads to a comparatively wide range in which coatings show increased porosity at decreased DE with larger particle sizes.

3.5. Effects of particle size in cold spraying and explosive powder compaction experiments

The influences of particle size and impact temperature on cold spray deposition were verified by spray experiments and explosive powder compaction using Cu and steel 316L powders of different size distributions. Experimentally determined critical velocities of different size cuts are summarized in Fig. 12 and expressed by Eqs. (9) and (10). Respective loading conditions in cold spraying were calculated by fluid dynamics. In explosive powder compaction, the critical velocities were determined by calculating the load required to obtain a transition from angular

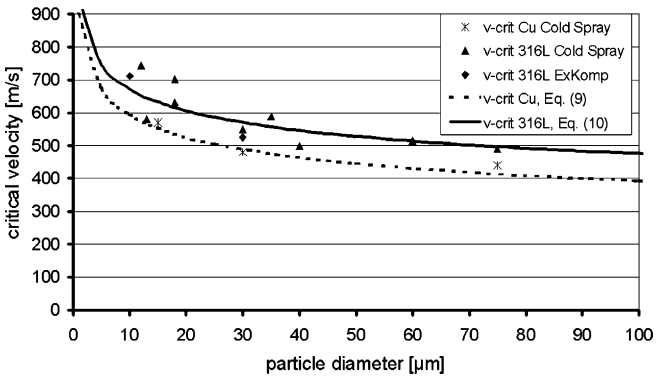

Fig. 12. Critical velocity measurements over particle diameter for copper and steel 316L. Approximation by Eqs. (9) and (10).

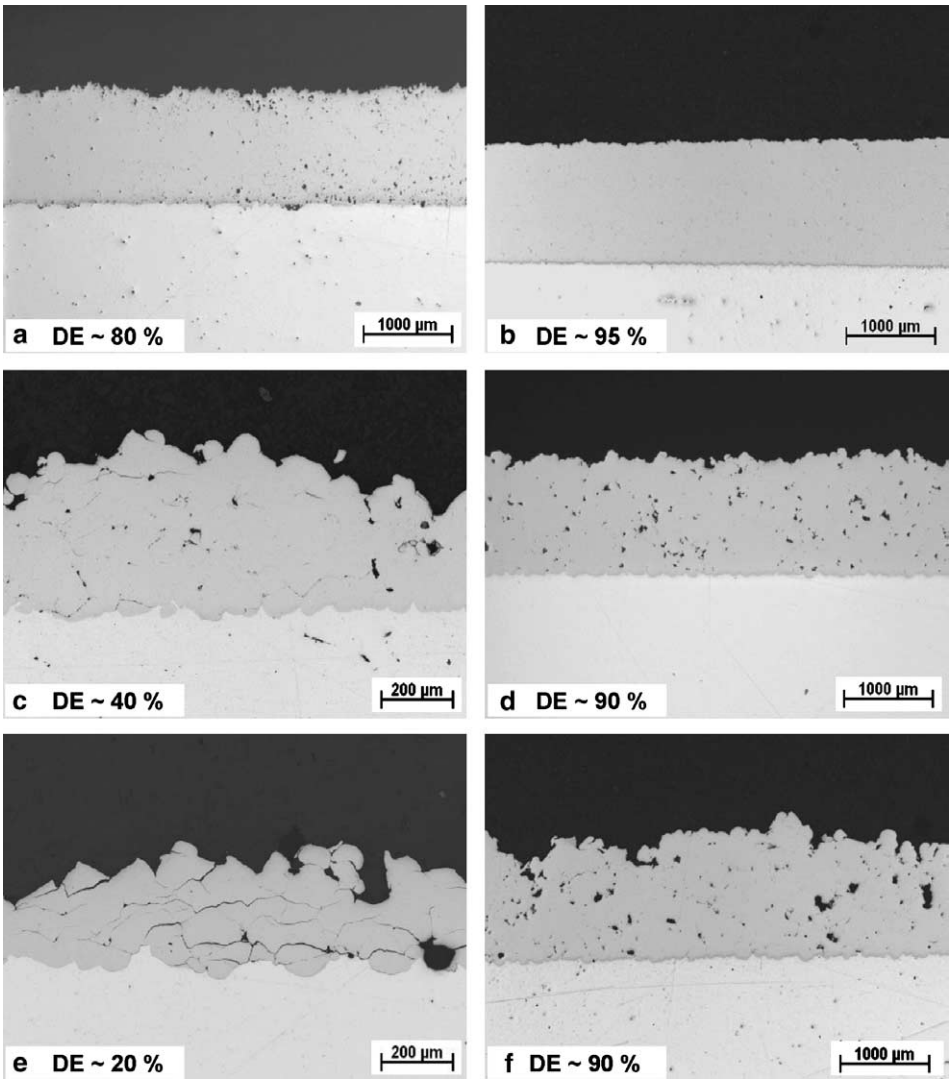

Fig. 13. Steel 316L sprayed with nitrogen (a,c,e) and helium (b,d,f). Size distribution: $-45+15$ μm (a,b), $-88+45$ μm (c,d), $-177+53$ μm (e,f).

microstructural features to parachute shapes and a respectively higher cavitation resistance. The results demonstrate that the critical velocity for both materials is decreasing with increasing particle diameter. A selection of cold-sprayed coating microstructures of steel 316L is shown in Fig. 13. With respect to the DE and low coating porosity, the optimum size distribution for steel 316L seems to be in the range of 15–45 μm ($-45+15$ μm). For smaller sizes (-22 μm) both, coating quality and DE decreased. For coarser particles of $-88+45$ and $-177+53$ μm, the DE was low when spraying with nitrogen. Spraying with helium resulted in a high DE, but also in an increased porosity with increased particle sizes.

As mentioned earlier, there might be various reasons for size effects, of which, due to the lack of data, only a couple can be described by modelling. The finite element simulations nicely demonstrate that for copper, heat conduction obviously dominates the size effect. Including heat conduction in the modelling for steel 316L does not lead to satisfactory results, just requiring other explanations with respect to powder quality or different deformation mechanisms under high strain rates. Apart from cold spray experiments, analyses of shock wave compacted samples supplied sufficient information concerning possible reasons.

For steel 316L, in particular, shock compaction experiments showed that there are significant and unexpected differences in particle bonding and particle deformation pattern comparing the fine powder (-22 μm) with the coarser powder ($-177+53$ μm) under same loading conditions, Fig. 14. Fine particles are significantly less deformed than coarser particles and only at substantially higher loads show the parachute deformation pattern together with shear instabilities and bonded interfaces. As assessed by cavitation tests, compacts processed with finer steel 316L powders show worse particle–particle adhesion than those processed with coarser powders. One possible explanation for the remarkably large size effect of steel 316L might be given by powder impurities or morphologies. Since SEM investigation of the 316L powder showed that all particles have a regular spherical morphology and a

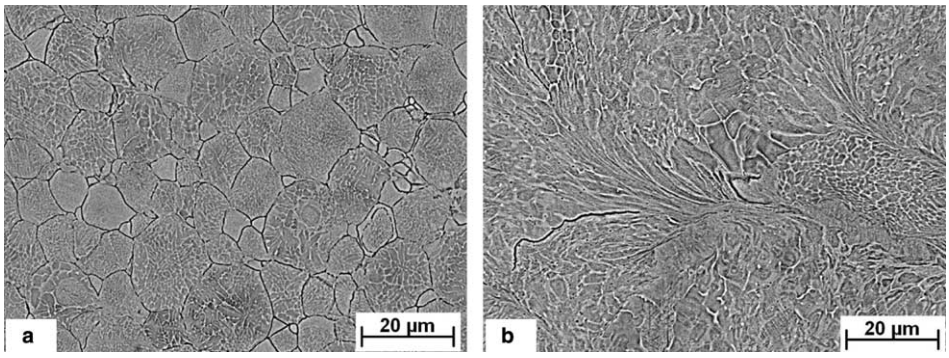

Fig. 14. Shock consolidated steel 316L powders of different size distributions: −22 µm (a), −177 + 53 µm (b), SEM-pictures of etched cross-sections. Under same loading conditions the particle–particle interfaces of the coarser powder show a higher chemical stability and a similar contrast as normal grain boundaries.

fine dendritic microstructure, different morphologies were excluded as a possible reason. Analyses of the composition showed that the finer particles (−22 µm) have eight times higher nitrogen content than the coarser ones (−177 + 53 µm). But even for the −22 µm powder the impurity content is quite low, as shown in Table 2. Micro-hardness measurements proved that the effect of these impurities is negligible with respect to the static material strength. The particle hardness and the hardness of respective compacts are only increased by less than 10%, Table 2. According to calculations, this would make a difference in critical velocity of only 20–30 m/s, but the experimentally determined difference in critical velocity is more than 150 m/s. Thereby it can be excluded that this could be the result of a higher static strength. The worse bonding quality could be related to the shorter time scale for welding, as mentioned before (3.1), but the different deformation pattern can only be explained by an increase in dynamic strength for small dimensions.

Differences in the bonding quality of the copper coatings were also determined by TCT-tests (see Section 2.4). An extract of the results is given in Table 3. This shows that under comparable impact conditions, coatings sprayed with coarser particles show a significantly higher strength than coatings sprayed with finer particles. An increase in particle impact temperature additionally improves the particle–particle adhesion in a significant range (Table 3). These results confirm the findings of modelling concerning the effect of particle size and temperature on particle bonding (see Sections 3.1–3.3).

Table 2
Chemical analysis and hardness values for 316L powders

Particle size distribution (µm)	O_2 (ppm)	N_2 (ppm)	Powder hardness HV0.01	Compact hardness HV0.1
−22	53	144	201	440
−177 + 53	12	18	185	400

Table 3
Results of coating tensile test, copper coatings

Particle size distribution (µm)	Calculated particle impact velocity (m/s)	Calculated particle impact temperature (°C)	Tensile strength (MPa)
−25 + 5 (15)	650	170	85
−38 + 10 (25)	650	170	130
−38 + 10 (25)	600	300	150

Experimentally determined critical velocities of different metals were already shown in Fig. 8 and demonstrate significant differences with respect to material properties which can be mainly attributed to the complex interplay of material density, deformation behaviour and thermal material properties. The comparison to calculated values reveals that the given formula at least for the considered powder size of 25 µm can supply a quite good estimation even for materials with quite different mechanical properties and melting temperatures. With respect to applications, it might be worth noting that Cu and Ta have quite similar critical velocities, despite the large difference in melting temperatures. Tin is having a quite low critical velocity due to the low strength and the low melting temperature.

3.6. Deposition and penetration by single impacts of 20 mm metal spheres

To study the extreme end of the effect of size on critical velocities, impact experiments with 20 mm balls of Cu, low carbon steel (1.0037) and Al were performed on substrates of the same materials or combinations of that. Since in that type of experiments, velocities of particles are directly measured, these single impacts supply well defined information concerning high strain rate deformation. Moreover, that method allows an easy investigation of requirements for bonding.

For the example of a low carbon steel ball impacting on a low carbon steel substrate, just not achieving bonding conditions, Fig. 15 shows macro-images and micrographs of the deformed surface. Attaining an impact velocity of 460 m/s, the steel ball bounced back from the substrate, leaving a typical deformation pattern of conditions close to the critical velocity. The macro image (Fig. 15(a)) shows that formation of material jets already occurs at the outer rim of the impact crater. The detailed view of the interface

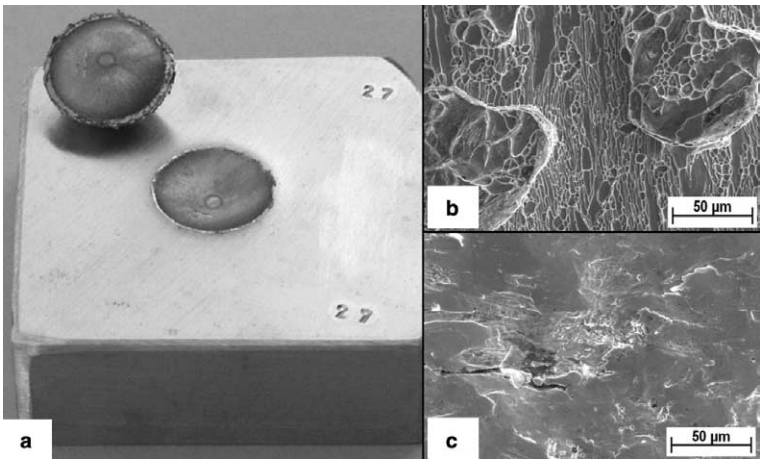

Fig. 15. Impact of low carbon steel ball to low carbon steel plate with 460 m/s. Macro picture of deformed ball and impact crater (a). The ball bounced back because of insufficient bonding. Dimple fracture at the crater sides (b), no indication for bonding at the south-pole (c), SEM-pictures.

morphologies by SEM reveals that areas close to the crater sides show a dimple pattern of ductile fracture (Fig. 15(b)), whereas the area around the centre at the south pole shows less plastic deformation and no bonding at all (Fig. 15(c)). Nevertheless, even when shear instabilities had already occurred, the extent of the bonded area was not large enough to resist the bouncing-back forces. These findings concerning deformation pattern are in good agreement with results from finite element analyses, showing bonded areas at the sides of the impact crater and not at the south pole (compare Fig. 2(b)).

For the same material type of impacting sphere and substrate, the experimentally determined critical velocities are shown and compared to calculated values in Fig. 8(a) and (c). For calculation, Eq. (8) was used with $F_1 = 0.45$ and $F_2 = 0.12$. Because the size effect is not included in Eq. (8) the values of F_1 and F_2 have to be different from those determined for the 25 µm particle. The comparison to the three orders of magnitude smaller cold spray particles demonstrates that the critical velocity is significantly lower for macroscopic impacts. As shown in Fig. 11, the size effect is very prominent for particles with less than 50 µm in diameter and shows a slight decrease leading to a saturation limit for bigger particle sizes.

For the material combination of Cu balls impacting on low carbon steel substrates, the whole range from below critical velocities for bonding up to velocities causing dynamic erosion was tested to demonstrate the effect on

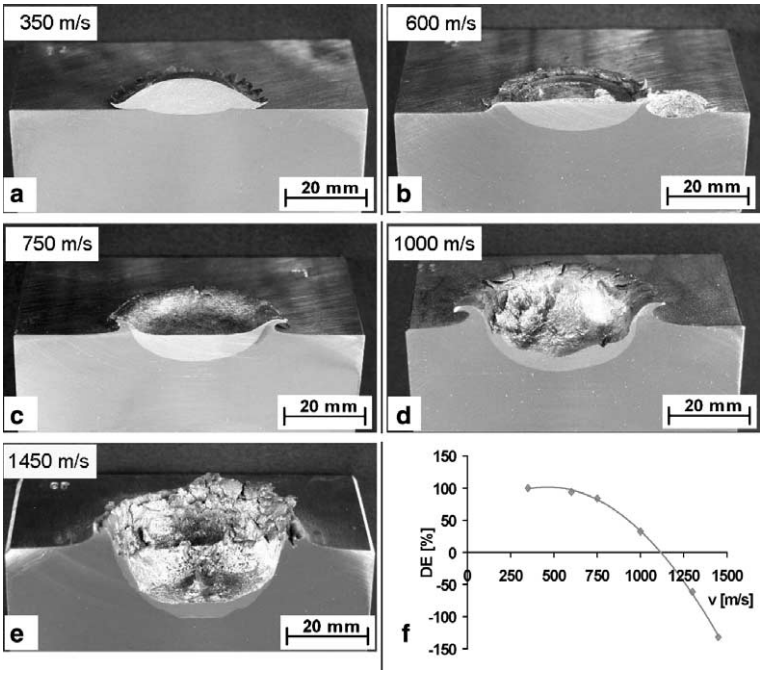

Fig. 16. Macro pictures of cross-sections of copper ball impacts to low carbon steel plates with different velocities. Diagram (f) shows the determined mass balance (DE) over impact velocity.

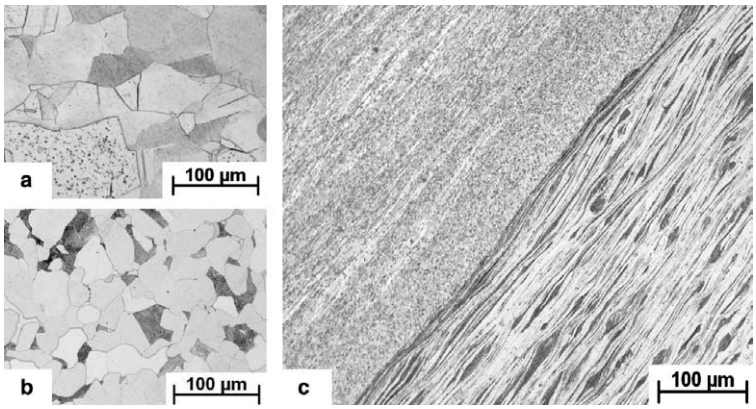

Fig. 17. Microstructure of a copper ball impact at a low carbon steel plate with 800 m/s (c). Initial microstructure of copper ball (a) and steel plate (b).

bonding and deformation pattern. Five cross-sections of this series are shown in Fig. 16. The results show that bonding of Cu on steel starts at velocities of about 350 m/s and that a very narrow welded bond zone is sufficient to withstand back striking forces (Fig. 16(a)). The extent of well bonded areas reached optimum conditions at about 600–750 m/s (Fig. 16(b) and (c)). Above this velocity range, an increasing loss of material is obtained with regard to the mass of the impacting sphere and the mass of the steel substrate. At 1150 m/s, there is no more deposition and an impact velocity of 1450 m/s causes an erosion of 140% with respect to the initial mass of the copper ball (Fig. 16(e)). Fig. 16(f) shows the experimentally determined DE over velocity for that type of single impact. These data were used to calibrate Eq. (8) for the calculation of v_{erosion} as shown in Fig. 9.

Cross-sections of the initial microstructures and the highly deformed microstructures after an impact with 800 m/s of a copper ball and the steel substrate are compared in Fig. 17. In the steel substrate, at areas of shear instabilities (sides of the crater), grains close to the bond zone are highly elongated and show a strain of 10 or even more. In such highly strained regions, the impacted copper particle shows recrystallization over a width of 50–100 µm from the bond line, caused by substantial thermal influences in the bond zone to the steel, which agrees with calculations. Shear test samples prepared from this 20 mm impact of Cu on steel, obtained at a velocity of 800 m/s, showed a shear strength of 200 MPa at the sides of the impact crater, which is as high as the shear strength of work hardened copper. Here most of the interfaces show ideal bonding, except of the 'south-pole-region' of the particle, encompassing an area of less than 20% of the total interfacial area. This is yet another indication that bonding does not occur at the point of highest pressure by adiabatic compression.

4. Summary and conclusions

In the present investigation, spray experiments, explosive powder compaction and impact tests with 20 mm balls were combined with modelling of impact phenomena to study general influences on bonding in cold spraying. Calculations and experimental results demonstrate that size effects in impact dynamics can have a significant influence on the critical velocity, which has to be exceeded for bonding, and thus on the amount of bonded area and coating quality. The results obtained for copper and steel 316L clearly demonstrate that critical velocities decrease with increasing particle size, which can be attributed to effects by heat conduction or strain rate hardening, respectively. Moreover, the experimental results were fitted by a simple, but physically sensible expression, allowing convenient estimation of critical velocity for a broad range of metallic materials. Based on that analysis, a simple expression was supplied which allows an easy estimation of critical velocities for quite different metallic materials. Since particle penetration causing erosion can play a role for very high impact velocities, respective limits were also included in that description. By defining the influences of particle temperature and velocity on bonding, a parameter window for cold spray deposition can be developed, which for successful spray experiments must be met by the respective particle impact conditions. With respect to attainable particle velocities and critical velocities, an optimum range of powder size distribution can also be predicted to achieve maximum coating qualities.

The generalized approach developed in this study supplies the tools needed to predict optimum spray conditions and required powder size cuts for successful cold spraying of various materials. Therefore, the number of time consuming and costly experiments can be significantly reduced to tune cold spraying for a particular new material.

Acknowledgements

The authors thank Mr. Papesch and Mr. Bruemmer from the Technical Centre for Weapon and Ammunition of the Federal Armed Forces (WTD 91) for support in performing experiments of explosive powder compaction and ballistic impacts. The Deutsche Forschungsgemeinschaft supported part of this research under Grant No. KR 1103/3-3, which is gratefully acknowledged.

References

[1] Assadi H, Gärtner F, Stoltenhoff T, Kreye H. Acta Mater 2003;51:4379.

[2] Schmidt T, Gärtner F, Kreye H. High strain rate deformation phenomena in explosive powder compaction and cold gas spraying. In: Marple BR, Moreau C, editors. Proceedings of the ITSC 2003 held in Orlando. Materials Park (OH): ASM International; 2003. p. 9.

[3] Stoltenhoff T, Kreye H, Richter HJ. J Thermal Spray Tech 2002;11:542.

[4] Voyer J, Stoltenhoff T, Kreye H. Development of cold sprayed coatings. In: Marple BR, Moreau C, editors. Proceedings of the ITSC 2003 held in Orlando. Materials Park (OH): ASM International; 2003. p. 71.

[5] Grujicic M, Zhao CL, Tong C, DeRosset WS, Helfrich D. Mater Sci Eng 2004;368:222.

[6] Blazynski TZ. Explosive welding, forming and compaction. London: Applied Science Publishers; 1983. p. 219.

[7] Deribas AA. The problem of obtaining dense and strong compacts in explosive loading of powders. In: Murr LE, Straudhammer KP, Meyers MA, editors. Proceedings of the international conference on metallurgical and materials application of shock-wave and high-strain-rate phenomena (EXPLOMET '95). New York (NY): Elsevier Science B.V.; 1995. p. 23.

[8] Papyrin AN, Klinkow SV, Kosarev VF. Modelling of particle-substrate adhesive interaction under the cold spray process. In: Marple BR, Moreau C, editors. Proceedings of the ITSC 2003, Orlando. Materials Park (OH): ASM International; 2003. p. 27.

[9] Van Steenkiste T, Smith JR. J Thermal Spray Tech 2004;13:274.

[10] ABAQUS/Explicit 6.3 Manual. Hibbitt, Karlsson & Soerensen, Pawtucket, RI, USA; 2002.

[11] Carleone J. Am Inst Aeron Astron 1993;155:165. 223.

[12] Zukas JA. High velocity impact dynamics. New York (NY): Wiley; 1990.

[13] Tzou DY. ASME J Heat Transf 1995;117:8.

[14] Prümmer R. Explosivverdichtung pulveriger Substanzen. Berlin: Springer; 1987.

[15] Murr LE. Shock waves for industrial applications. New Jersey: Noyes Publications; 1988.

[16] Raybould D. J Mater Sci 1981;16:589.

[17] Morris DG. Mater Sci Eng 1983;57:187.

[18] Shang SS, Benson DJ, Meyers MA. J Phys 1994;IV,C8:521.

[19] Schwetzke R, Kreye H. Cavitation Erosion of HVOF Coatings. In: Berndt CC, editor. Proceedings of the 9th national thermal spray conference (NTSC '96). Materials Park (OH): ASM International; 1996. p. 153.

[20] Hammerschmidt M. Mikrostruktur und Eigenschaften von Explosivschweißungen. Düsseldorf: VDI; 1983.

[21] Smithells CJ. Metals reference book. 7th ed. Oxford: Butterworth-Heinemann; 1992.

[22] Pintat T. Werkstofftabellen der Metalle. 8. Auflage. Stuttgart: Alfred Kröner; 2000.

[23] Material properties data base: www.matweb.com.